

AD-A256 204



2

NAVAL POSTGRADUATE SCHOOL

Monterey, California



SE
OCT 21 1992
ED

THESIS

EFFECT OF THERMOMECHANICAL TREATMENTS
ON THE AGING RESPONSE OF CENTRIFUGALLY CAST
SILICON CARBIDE/ALUMINUM COMPOSITES

by

Christopher William May

June, 1992

Thesis Advisor:

Indranath Dutta

Approved for public release; distribution is unlimited

251450 4300
92-27473



UNCLASSIFIED

SECURITY CLASSIFICATION OF THIS PAGE

REPORT DOCUMENTATION PAGE				Form Approved OMB No 0704-0188	
1a REPORT SECURITY CLASSIFICATION UNCLASSIFIED			1b RESTRICTIVE MARKINGS		
2a SECURITY CLASSIFICATION AUTHORITY			3 DISTRIBUTION/AVAILABILITY OF REPORT Approved for public release; distribution is unlimited.		
2b DECLASSIFICATION/DOWNGRADING SCHEDULE					
4. PERFORMING ORGANIZATION REPORT NUMBER(S)			5. MONITORING ORGANIZATION REPORT NUMBER(S)		
6a. NAME OF PERFORMING ORGANIZATION Naval Postgraduate School		6b OFFICE SYMBOL (If applicable) Code ME	7a. NAME OF MONITORING ORGANIZATION		
6c. ADDRESS (City, State, and ZIP Code) Monterey, CA 93943-5000			7b. ADDRESS (City, State, and ZIP Code)		
8a. NAME OF FUNDING / SPONSORING ORGANIZATION		8b OFFICE SYMBOL (If applicable)	9 PROCUREMENT INSTRUMENT IDENTIFICATION NUMBER		
8c. ADDRESS (City, State, and ZIP Code)			10 SOURCE OF FUNDING NUMBERS		
			PROGRAM ELEMENT NO	PROJECT NO	TASK NO
					WORK UNIT ACCESSION NO
11 TITLE (Include Security Classification) EFFECT OF THERMOMECHANICAL TREATMENTS ON THE AGING RESPONSE OF CENTRIFUGALLY CAST SILICON CARBIDE/ALUMINUM COMPOSITES (UNCLAS)					
12 PERSONAL AUTHOR(S) Christopher W. May					
13a TYPE OF REPORT		13b TIME COVERED FROM _____ TO _____	14 DATE OF REPORT (Year, Month, Day) June 1992		15 PAGE COUNT 44
16 SUPPLEMENTARY NOTATION The views expressed in this thesis are those of the author and do not reflect the official policy of the Department of Defense or the U.S. Government					
17 COSATI CODES			18 SUBJECT TERMS (Continue on reverse if necessary and identify by block number)		
FIELD	GROUP	SUB-GROUP	Aluminum Matrix Composites		
19 ABSTRACT (Continue on reverse if necessary and identify by block number) Differential scanning calorimetry was conducted using centrifugally cast monolithic A356 aluminum material and 26 volume percent silicon carbide (SiC) particle reinforced A356 aluminum matrix composite material in as-cast, cast and rolled, and cast and extruded conditions. Electrical resistivity and matrix micro-hardness measurements during isothermal aging treatments were also conducted. the effects of thermo-mechanical processing and SiC particle additions on the mechanical properties and aging kinetics of the metastable phases in each material were studied.					
20 DISTRIBUTION/AVAILABILITY OF ABSTRACT <input checked="" type="checkbox"/> UNCLASSIFIED/UNLIMITED <input type="checkbox"/> SAME AS RPT <input type="checkbox"/> DTIC USERS			21 ABSTRACT SECURITY CLASSIFICATION Unclassified		
22a NAME OF RESPONSIBLE INDIVIDUAL Professor I. Dutta			22b TELEPHONE (Include Area Code) (408) 646-2581		22c OFFICE SYMBOL ME/Du

Approved for public release; distribution is unlimited.

**EFFECT OF THERMOMECHANICAL TREATMENTS
ON THE AGING RESPONSE OF CENTRIFUGALLY CAST
SILICON CARBIDE/ALUMINUM COMPOSITES**

by

**Christopher William May
Lieutenant, United States Navy
BSME, Tulane University, 1984**

Submitted in partial fulfillment
of the requirements for the degree of

MASTER OF SCIENCE IN MECHANICAL ENGINEERING

from the

NAVAL POSTGRADUATE SCHOOL

June 1992

Author:



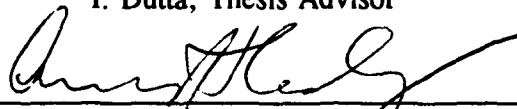
Christopher W. May

Approved by:



I. Dutta, Thesis Advisor

I. Dutta, Thesis Advisor



Anthony Healey, Chairman

Anthony Healey, Chairman
Department of Mechanical Engineering

ABSTRACT

Differential scanning calorimetry was conducted using centrifugally cast monolithic A356 aluminum material and 26 volume percent silicon carbide (SiC) particle reinforced A356 aluminum matrix composite material in as-cast, cast and rolled, and cast and extruded conditions. Electrical resistivity and matrix micro-hardness measurements during isothermal aging treatments were also conducted. The effects of thermo-mechanical processing and SiC particle additions on the mechanical properties and aging kinetics of the metastable phases in each material were studied.

Available For	
DTIC (A) (U)	<input checked="" type="checkbox"/>
DTIC (S) (U)	<input type="checkbox"/>
DTIC (S) (U)	<input type="checkbox"/>
By _____	
Date _____	
Availability Codes	
Dist	Avail. and/or Special
A-1	

TABLE OF CONTENTS

I. INTRODUCTION	1
A. METAL MATRIX COMPOSITES (MMCs)	1
B. AGING BEHAVIOR AND MICROSTRUCTURAL EVOLUTION . .	3
1. Microstructural Evolution in Al-Mg-Si Alloys	3
2. Impact of Reinforcements on Aging Behavior	4
C. RESEARCH OBJECTIVE	5
II. DESCRIPTION OF MATERIALS	7
III. EXPERIMENTAL PROCEDURE	8
A. OPTICAL QUALITY POLISHING	8
B. HARDNESS TESTING	8
C. DIFFERENTIAL SCANNING CALORIMETRY	9
D. RESISTIVITY	11
E. TENSION TESTING	11
IV. RESULTS AND DISCUSSION	12
A. MECHANICAL PROPERTIES AND MICROSTRUCTURE	12

B. EFFECT OF REINFORCEMENTS AND PROCESSING ON	
AGING	21
1. Microhardness	21
2. Differential Scanning Calorimetry	23
a. Effect of SiC Particle Addition on the Matrix Aging	
Response	24
b. Effect on Post-Fabrication Processing on the Matrix Aging	
Response	26
3. Resistivity	29
V. CONCLUSIONS	33
LIST OF REFERENCES	35
INITIAL DISTRIBUTION LIST	37

I. INTRODUCTION

A. METAL MATRIX COMPOSITES (MMCs)

The enhanced material properties available by forming composites has been known for many years, and polymer matrix composites have grown common in use for sporting equipment. The widespread use of composite materials for useful engineering applications has been limited by cost of fabrication, typically a powder metallurgy (PM) technique, where the reinforcement and a powdered matrix metal are compressed under high heat and pressure.

Due partly to the limitations on size for PM processed parts, interest in cast MMCs has increased recently as a cost-effective way to benefit from the increased strength-to-weight ratio, stiffness, temperature stability, and fatigue characteristics of metals reinforced with ceramic fibers, whiskers, or particles. Discontinuous ceramic reinforcements can be pre-mixed with the molten metal prior to casting, allowing the use of common casting equipment and techniques. In particular, centrifugal casting has emerged as a viable way to produce large near net shape parts, and is particularly suited to producing bodies of rotation. It involves injecting the melt into a heated thin wall mold spinning at a high rate of speed. The high 'g'-forces experienced by the melt yield advantages similar to squeeze casting, and relatively rapid cooling rates can be achieved which would not be possible with a standard large casting mold. Rapid cooling of castings also results in a high productivity.

Problems in casting include poor wetting of the reinforcement by the molten metal, and inhomogeneous reinforcement distribution due to flocculation, resulting in poor as-cast microstructures and properties [Ref. 1]. As a result, post fabrication thermomechanical processing (TMP), such as hot isostatic pressing (HIPing) or extrusion, is usually required. Although fiber and whisker reinforced composites provide the greatest gains in mechanical properties along their longitudinal axes, they are also anisotropic in nature and their properties suffer greatly during post-casting TMP due to fiber or whisker breakage. Particulate reinforced metals have shown great promise as an economical and relatively isotropic solution.

Prior research [Refs. 2-5] has shown significant improvement in the mechanical properties of metal matrix composites with TMP. A more homogenous distribution of reinforcement particulates has been shown to increase ductility due to a lessened degree of localized deformation [Ref. 2]. It is also known that a homogenous particulate distribution in a processed composite microstructure gives rise to more uniform nucleation sites, due to particle stimulated nucleation [Ref. 3], resulting in a fine grain /subgrain structure and a higher ductility.

In addition to sealing pores and redistributing the reinforcement particles, thermomechanical processing has been shown to cause an accelerated aging response in precipitation hardenable aluminum alloys. Papazian [Ref. 6] showed that deformation of an 2219 Al alloy increased the rate of precipitate formation, and that this rate continued to increase with increasing deformation. This acceleration in precipitation was thought to be most likely due to the presence of a high dislocation density, which provide

high diffusivity paths (pipe diffusion along the dislocations). Therefore, it is reasonable to assume that such effects of TMP will also be present in aluminum matrix composites with precipitation hardenable matrices.

B. AGING BEHAVIOR AND MICROSTRUCTURAL EVOLUTION

1. Microstructural Evolution in Al-Mg-Si Alloys

Aluminum A356 is an age hardenable alloy which contains the following nominal composition of alloying elements [Ref. 6]:

TABLE I: COMPOSITION OF A356 ALUMINUM

Si	Mg	Cu	Fe	Ti	Mn	Zn	others
6.5 to 7.5	0.45 to 0.25	0.20 max	0.20 max	0.20 max	0.10 max	0.10 max	0.15 max total

Age hardening behavior in the various Al-Mg-Si alloys has been extensively studied, yet there has not yet been agreement among the many authors of the sequence, composition, and morphology of the phases.

In their studies, both Thomas [Ref. 7] and Lutts [Ref. 8] concluded that the first stage of precipitation from a supersaturated solid solution was a needle shaped precipitate, while Cordier and Gruhl [Ref. 9] determined that the early GP zones were approximately spherical. Cordier and Gruhl did not observe the needle like particles until the region of peak hardness.

Ceresara *et al.* [Ref. 10] found that in alloys which form Mg_2Si , Si in excess of that required for Mg_2Si formation did not alter the aging process, but did alter the

kinetics (i.e., it increased the process rate) and thermodynamic factors (i.e., it created smaller, more dispersed zones). Kovacs *et al.* [Ref. 11] found that this Si is the first to precipitate, and that Mg and Si atoms then precipitate on the Si vacancy clusters. Dutta and Allen [Ref. 12] also showed spherical Si clusters forming first, followed by fine, near-spherical GP I zones of an unresolved shape. The GP I zone formation was followed by the precipitation of needle-like GP II, or β'' . A rod-like β' was the next to precipitate, followed by the equilibrium phase of β platelets.

2. Impact of Reinforcements on Aging Behavior

The reinforcements used to make MMCs are typically high melting point, relatively inert materials. As such, the reinforcements would not be expected to significantly alter the chemistry of the matrix alloy. Although in Al-SiC composites the chemistry of the Al-SiC interface is usually not complicated, reinforcement particles have long been known to have significant effect on the aging behavior of the composite matrix [Refs. 13-18]. Experiments have shown that Al matrix composites reach peak hardness in one-half to one-third the time required for the monolith, i.e. matrix alloy, to reach peak hardness [Refs. 13 and 14].

From previous investigations into this phenomenon, two mechanisms have been generally accepted to explain the occurrence of accelerated aging in MMCs. Both mechanisms can be attributed to the thermal mismatch strain between the reinforcement and the matrix. This strain occurs as a result of a mismatch between the coefficients of thermal expansion (CTE) of the matrix and reinforcement.

Upon cooling the composite from fabrication temperature, the CTE mismatch (ΔCTE) results in large local strain fields around the reinforcements. These strain fields are relaxed by the formation of dislocations in the matrix. These dislocations serve as heterogeneous nucleation sites for second phase precipitation. As a result of having many more nucleation sites, the MMC ages more quickly [Refs. 13 and 15]. Additionally, the matrix dislocation in MMCs also enhance aging kinetics via increased pipe diffusion at low temperatures [Ref. 19].

In the second mechanism, the diffusion of solute atoms through the matrix is enhanced by the stress fields generated by the CTE mismatch. Although this mechanism has been modeled and theoretically shown to provide a comparable precipitation rate for a range of reinforcement volume percent and morphology, experimental evidence has shown that the dislocation model dominates. [Ref. 16]

C. RESEARCH OBJECTIVE

Many studies have been published on the mechanical properties of composites, and also on the aging kinetics of age-hardenable MMC's. Most of the papers dealing with aging kinetics deal primarily with materials formed using the powder metallurgy process, and have whisker reinforcements vice particulate reinforcements.

Little systematic study of the effect of post-fabrication TMP on cast particulate reinforced composites has been conducted. McNelley and Kalu [Ref. 2] showed some success in increasing strength and ductility with specific thermomechanical treatments on a 6061 Al- Al_2O_3 composite, and Dutta *et al.* [Ref. 1] showed an increase in both strength

and ductility with increasing TMP in a commercially cast aluminum alloy 5083 reinforced with 10 v/o SiC particles. Due to the large ratio of CTE's between Al and SiC (about 10:1), accelerated aging is also expected to occur. It is unclear how TMP such as extrusion will affect the aging kinetics.

The purpose of the present work is to study the effect of thermo-mechanical processing, such as HIPing and extrusion, on centrifugally cast aluminum matrix composites. The main areas of interest include the relationship between processing and mechanical properties, and the effect of processing on the matrix aging kinetics.

II. DESCRIPTION OF MATERIALS

The aluminum alloy and composite materials used in this study were received from the Naval Surface Warfare Center, Silver Spring, MD. The material was centrifugally cast as previously described under proprietary conditions. The monolithic material was a commercial grade A356 Al alloy; the composites were reinforced with 26 volume percent SiC particles. The particles were roughly spherical with an average diameter of 5 μm .

As-cast material as well as material which had been HIPed (670 K, 30 ksi, 2 hrs) were received in the form of machined flat-bar tensile samples with a nominal gage length of 31.75 mm (1.25 inch), with the sample axis aligned along the tube length. Material which had been co-extruded (625 K, 3.5:1 reduction) was received in the tube form, from which sub-size flat-bar tensile samples with a nominal gage-length of 12.7 mm (0.5 inch) and having the same orientation as the as-cast and HIPed samples were machined. Several as-cast flat-bar samples were also rolled (625 K, 3 passes, overall reduction 3.5:1) to allow for additional data for TMP comparison.

All samples not processed in an as-received condition underwent an eight hour homogenization heat treatment at 813 K.

III. EXPERIMENTAL PROCEDURE

A. OPTICAL QUALITY POLISHING

Polishing of an Al-SiC composite material presents challenges due to both the extreme variation in hardness between the matrix metal and the reinforcement, and the brittleness of the reinforcement. Sample polishing was started with a standard roll grinder and sanding papers ranging from 240-600 grit, using kerosene or soapy water as a lubricant instead of water. Care was taken to use only light pressure on the sample so as not to break or tear out particles. The samples were then successively wheel polished on a low nap (Buehler Texmet) polishing cloth with 45, 15, and 3 micron diamond paste using DP Red as a lubricant. Final polishing was on the Texmet cloth using 1 micron diamond paste and Buehler Metadi fluid, followed by a colloidal silica polishing suspension. The colloidal silica polishing was very light, as it tended to preferentially wear the aluminum matrix, leaving the SiC particles protruding.

B. HARDNESS TESTING

The microhardness measurements of the Al-SiC composite were obtained using a Buehler Micromet Vickers Microhardness Tester with a 25 gram load. The 25 gram load was used to ensure the entire indentation would be contained in the matrix area between particles, and to minimize effects from sub-surface particles. Prior to the homogenization heat treatment, samples were optically polished, then wrapped in

aluminum foil to help prevent oxidation and facilitate handling. All samples were homogenized in a horizontal tube furnace with an inert atmosphere at 813 K for 90 minutes, then vigorously quenched in ice water.

After quenching, samples were aged at 428 K in a convection oven for various times before again being quenched in ice water. After restoring the optical polish, an average of at least six readings were taken from each aged sample. Care was taken to ensure that the indenter was hitting only the matrix material but that it was close enough to the reinforcing particles so that their effects could be felt. The results of the hardness measurements were then converted to a Vickers hardness number (VHN) using tables provided with the tester.

C. DIFFERENTIAL SCANNING CALORIMETRY

The energy released during (or required for) precipitation reactions were measured using a Perkin-Elmer Model 7 Differential Scanning Calorimeter (DSC). The DSC was equipped with an intercooler for sub-ambient operation, and a glove box to minimize condensation on the sample chamber. Approximately 5mm samples were cut from both composite and monolithic stock using electric discharge machining. The samples were then hand sanded to approximately 40 mg and weighed using an analytical balance. After the homogenization heat treatment, and quenching as for the microhardness testing, the sample was dried and encapsulated in a sample pan, then placed into the DSC within three minutes of removing the sample from the quench bath.

An empty sample pan was used in the reference chamber for all runs; all test were preceded by a baseline using empty sample pans in the DSC chambers, which was subtracted from the test curves. All tests were run with the following parameters:

- Lower Temperature: 278 K
- Upper Temperature: 848 K
- Heating Rate: 10 K / minute
- Sample Chamber/Glove Box Purge Gas: Nitrogen 95% pure (drying towers were added prior to apparatus)

Several samples of each processed condition were scanned to ensure reproducibility of results. After a scan was completed, the heat flow versus temperature data was converted to heat capacity versus temperature using the following equation:

$$\frac{\text{Heatflow (W)}}{\text{Scanrate } (\frac{K}{s})} \cdot \frac{1}{\text{moles Al}} = \Delta C_p \left(\frac{J}{K \cdot \text{mole}} \right)$$

Data from the materials was normalized by the mass of the aluminum alloy. Volume percent of aluminum alloy was first converted to mass percent, then multiplied by the weight of the sample. Each data set was then divided by the appropriate mass to alloy for normalized comparisons.

D. RESISTIVITY

The changes in resistivity during isothermal aging of the test material were measured using the same experimental setup as Harper [Ref. 17]. Test strips were first given a homogenization heat treatment, followed by quenching into ice water. After a sample strip was taken from the ice bath, it was quickly dried and placed into the jig, which had been soaking in the oven stabilized at the aging temperature. A constant current of 0.5 amperes was passed through the sample strip; the resultant voltage drop across the sample was digitally sampled throughout the test period, and the resistivity was then calculated on the monitoring personal computer. Data was sampled in four intervals at a rate appropriate for the test temperature, and was collected using an automated data acquisition system.

E. TENSION TESTING

Tensile coupons were tested at ambient conditions on an Instron Model 6027 Tensile Testing machine. Coupons were tested in both as received and peak aged condition to failure, using a constant strain rate of 0.250 mm/minute. Strains were measured with a strain gage edge extensometer equipped with knife edges. Standard flat tensile coupon geometry as described in section II was used; the as cast and HIPed samples had a gage length of 1 inch, while the extruded samples had a gage length of ½ inch. Yield strength was calculated based on the standard 0.2% offset.

IV. RESULTS AND DISCUSSION

A. MECHANICAL PROPERTIES AND MICROSTRUCTURE

Figure 1 is a stress versus strain plot of the monolithic A356 samples tested in the as-received condition. A trend towards decreasing strength and greater ductility with processing is seen. The

same trend is seen in Figure 2, a stress versus strain plot of the composite samples. As expected, the MMC samples showed a greater stiffness and better strength than the monolithic alloy samples.

The HIPed materials, both monolith and composite, show a slight decrease in ultimate tensile strength (UTS) relative to the as cast samples, but a significant increase in

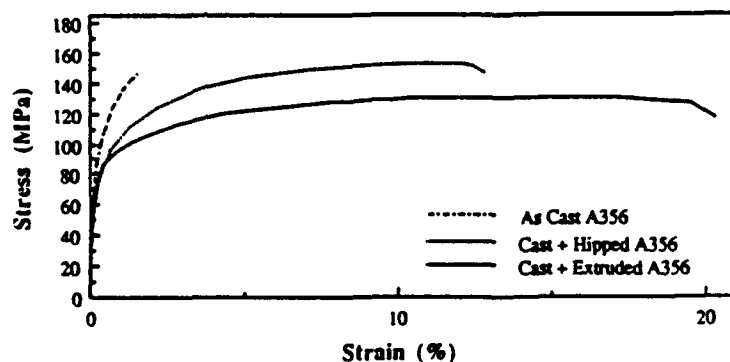


Figure 1: Stress-Strain Curve for Monolithic A356 Al Alloy in As Cast and Processed Conditions.

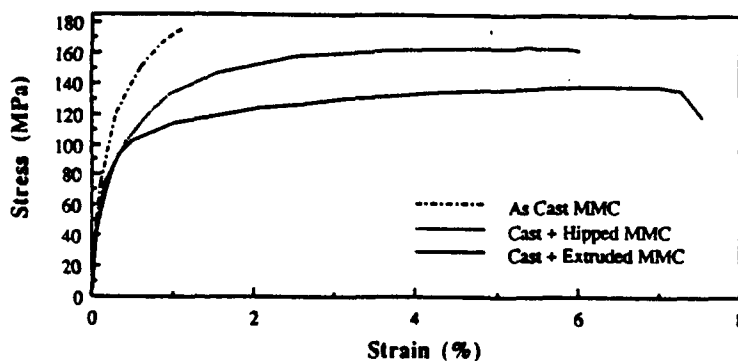


Figure 2. Stress-Strain Curve for A356 Al MMC in As Cast and Processed Conditions.

ductility. The extruded material shows an even lower UTS, but a large increase in ductility.

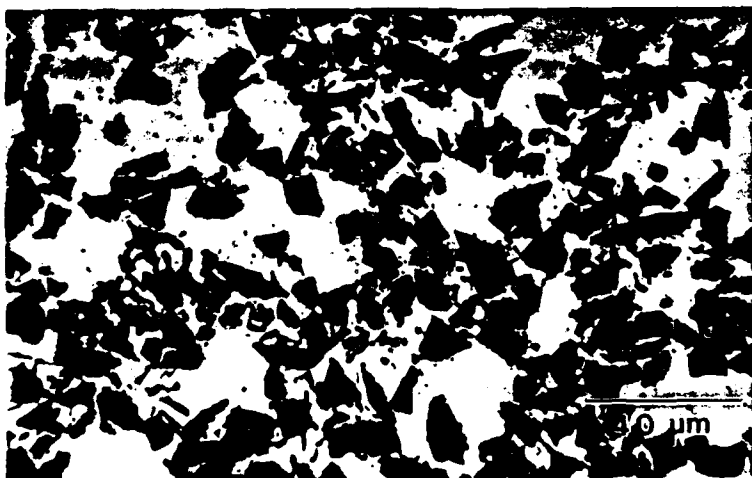
Figure 3 is a high magnification comparison of the microstructures of the monolithic and composite as cast material. In the monolith pictured in Figure 3a, large Si platelets can be seen. Comparing this with the composite shown in Figure 3b, the Si platelets in the composite matrix are notably refined, probably attributable to nucleation at particulate interfaces. In any case, the presence of SiC particulates results in refinement of the Si in the divorced eutectic. This refinement has a marked effect of fracture morphology, as can be seen from the fracture profiles in Figure 4. In the monolith of Figure 4a, secondary cracks can be seen in Si platelets away from the fracture surface. In the composite, Figure 4b, Si platelet refinement has occurred and alters the fracture morphology near the reinforcements. In areas free from reinforcements, such as the area at the top of Figure 4b, large Si platelets still form, and detract from fracture toughness.

Figures 5a and 5b are lower magnification optical micrographs of the as cast monolith and MMC. The large Si platelets are again seen in the monolith, while in the MMC the SiC particles are seen to be clustered. In areas this clustering has resulted in poor wetting by the matrix, resulting in poor bonding and interparticle void formation.

The microstructure of the HIPed material is shown in Figure 6. The monolithic material has little change other than interdendritic porosity closure. Interparticle void closure in the composite is also seen, although no change in reinforcement distribution is apparent.



(a)

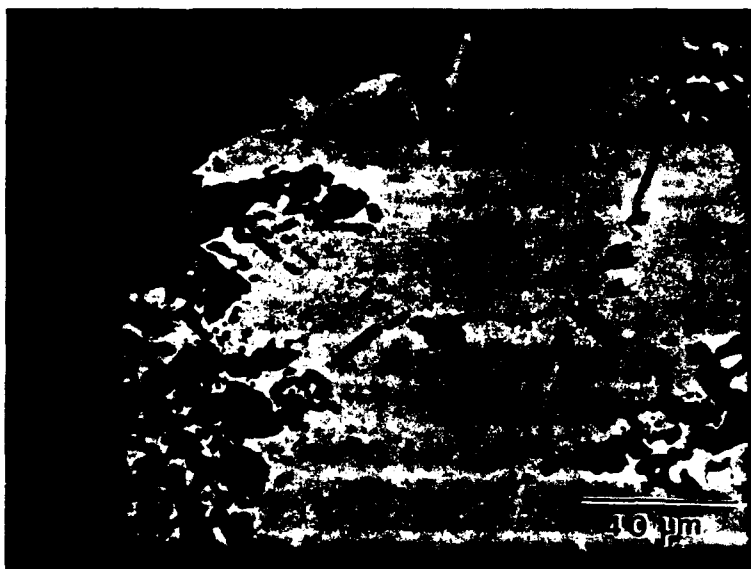


(b)

Figure 3. High Magnification Micrographs of As Cast Microstructure. (a) Monolith, (b) Composite.

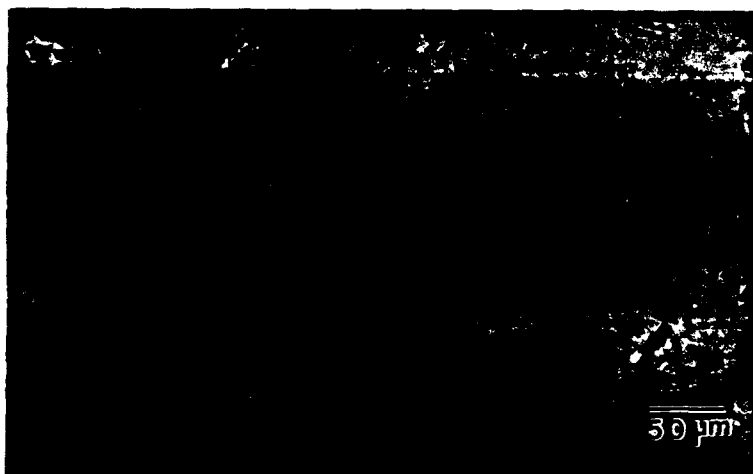


(a)

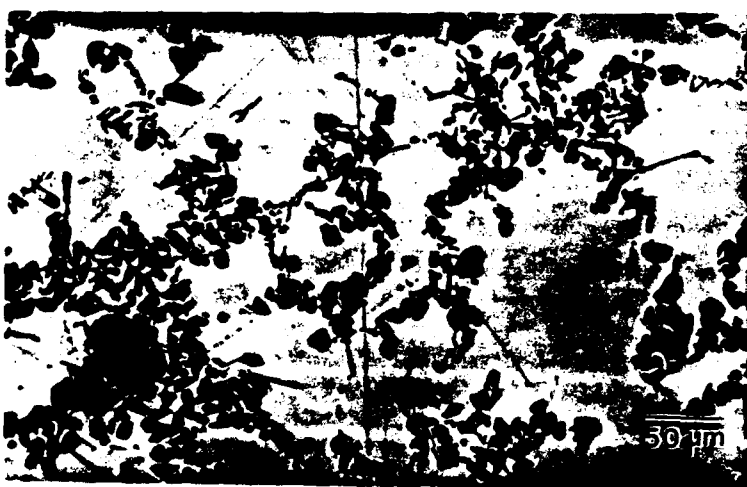


(b)

Figure 4. Comparison of Fracture Profiles for Monolithic and Composite Materials. Fracture of large Si platelets in monolith (4a) is not evident in reinforced regions of composite (4b) due to Si platelet refinement.



(a)

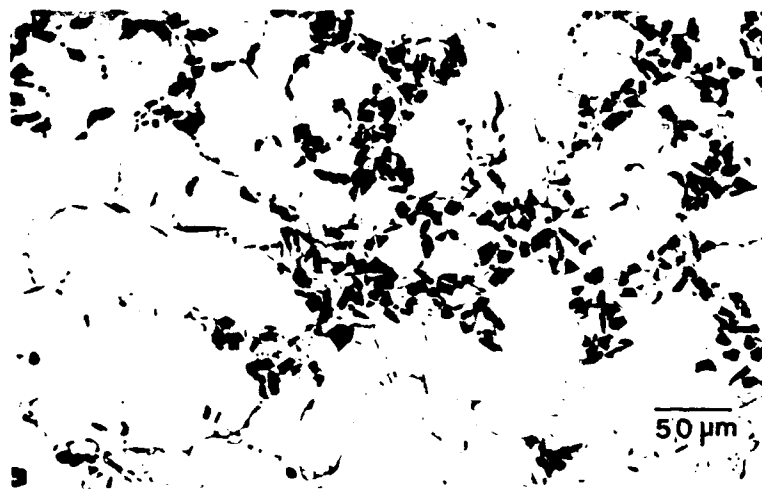


(b)

Figure 5. Microstructure of As Cast Material; (a) Monolith, (b) Composite.



(a)



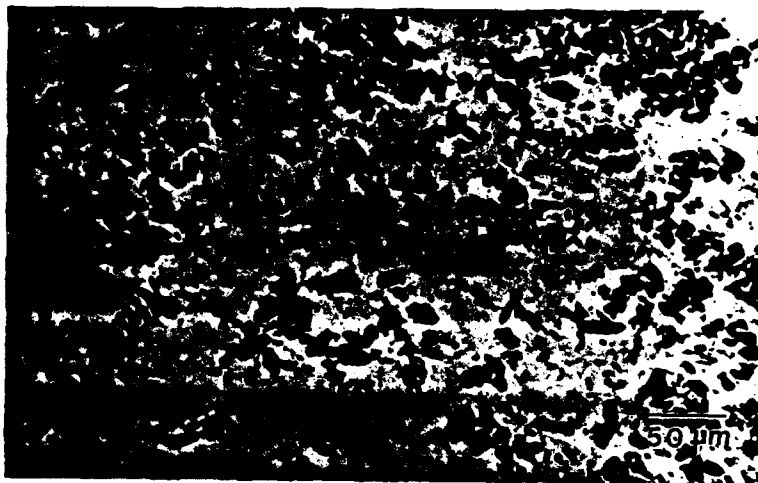
(b)

Figure 6. Microstructure of Hot Isostatically Pressed Material; (a) Monolith, (b) Composite.

Microstructure of the extruded material is shown in Figure 7. In the monolith, the Si platelets have been broken up somewhat and are more homogeneously distributed by



(a)



(b)

Figure 7. Microstructure of Extruded Material; (a) Monolith, (b) Composite.

the working, and the composite shows a more homogenous particle distribution, as well as a finer Si platelet distribution.

The HIPed monolith gains enhanced ductility from porosity closure, while the extruded material also has the Si platelets broken up during processing. The increase in ductility in the HIPed composite is due to porosity and interparticle void closure, and in the extruded MMC it is due to two reasons, one mechanical and the other microstructural. First, void closure and a more homogenous particulate reinforcement distribution due to the extrusion process has occurred. Second, refinement of Si platelets in the matrix due to the SiC particle addition has resulted in greater toughness.

The decrease in UTS in the processed samples is due to matrix over-aging during processing, as can be seen in the DSC thermogram of Figure 8, which depicts the variation in specific heat over the temperature range in which the transition precipitates β'' and β' form. It is observed that a decrease in precipitation with processing occurs; the curve for the extruded material shows virtually no precipitation, indicating that the material is

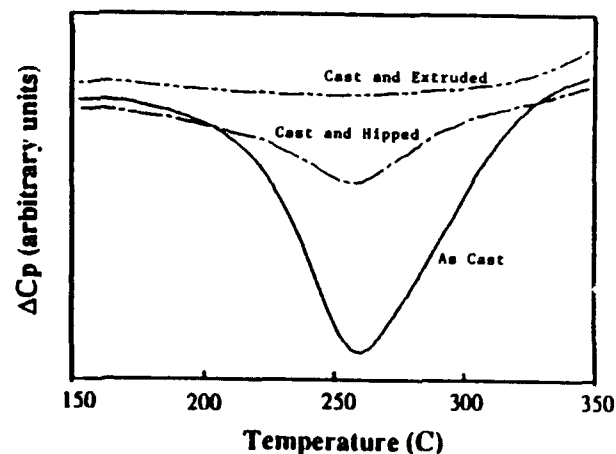


Figure 8. DSC Thermogram Showing Progressive Overaging During Material Processing.

completely over-aged. If the samples are solution heat treated and then aged to peak hardness, the results are significantly different, as can be seen in Figure 9. The MMC

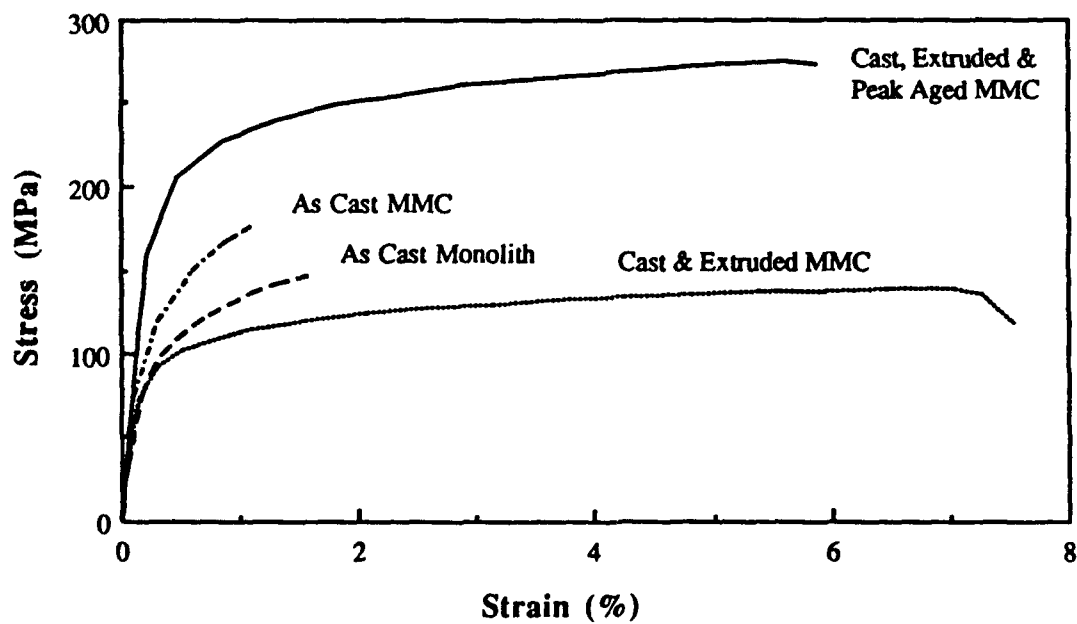


Figure 9. Stress-Strain Plot Showing Effects of Peak-Age Treatment After Processing.

which was extruded and then peak aged shows a marked increase in strength, while still retaining good ductility.

B. EFFECT OF REINFORCEMENTS AND PROCESSING ON AGING

1. Microhardness

Figure 10 shows the microhardness changes occurring during aging of the

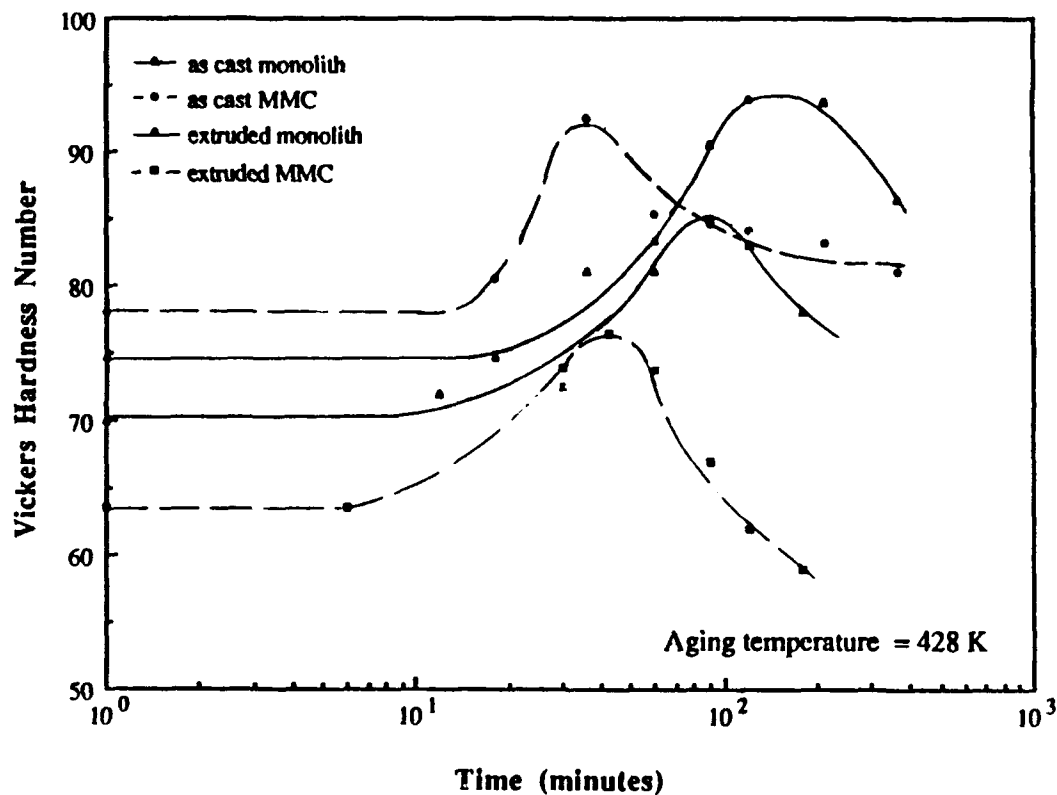


Figure 10: Matrix Microhardness Variation During Isothermal Aging at 428 K.

SiC_p reinforced MMC and the monolithic A356 Al in the as cast and the extruded conditions at 428 K. There are three interesting things to note from this figure. First, the matrix in the as cast condition has a higher initial hardness in both the monolith and

MMC, when compared to the extruded state. Secondly, both composite curves show accelerated aging compared to the monolithic materials. Finally, the effects of extrusion have affected the monolith and composite differently; extrusion has accelerated aging in the monolith while delaying it slightly in the composite.

It has been shown that the composite matrix shows refinement of Si platelets, although the effect of this on hardness is unclear. Generally, the refinement would be expected to increase dispersion strengthening, and hence hardness. However, TEM studies have shown that the Si platelets are heavily twinned, probably due to the ΔCTE between Si and Al during cooling from the processing temperature. This is shown in Figure 11, which also shows that the matrix and the platelets are highly dislocated. It is possible that the finer Si platelets in the extruded state twin more easily than the larger Si platelets in the as cast condition, thus reducing the plastic strain in the matrix. This would cause strength, and hardness, of the extruded materials to be lower than that of the as cast materials.

An alternative explanation for the softening observed due to extrusion is dislocation recovery into a subgrain structure, resulting in matrix softening. Thermo-mechanical processing resulting in a highly refined grain/subgrain structure has been observed in some MMC's [Refs. 4,5], and was attributed to prolific dislocation generation at the reinforcement-matrix interface and simultaneous recovery to the nearby grain/subgrain boundaries during straining, thus reducing the matrix dislocation density around the particulates.



Figure 11. TEM Micrograph of Si Platelets. Twinned Si platelets next to a SiC particulate, with the region next to the SiC particulate and the Si platelets heavily dislocated with well defined subgrains.

In the monolith, the accelerated aging observed in the extruded material relative to the as cast material is attributable to the increased average dislocation density generated during post-fabrication processing. In the MMC, the recovery of dislocations generated due to the CTE mismatch to grain/subgrain boundaries as mentioned above might be responsible for the slight delay in peak aging observed in Figure 10.

2. Differential Scanning Calorimetry

The DSC thermogram of the A356 aluminum alloy is shown in Figure 12. Four exothermic formation peaks are observed in the figure. The exothermic formation peaks correspond to the formation of new phases in the microstructure, and conform

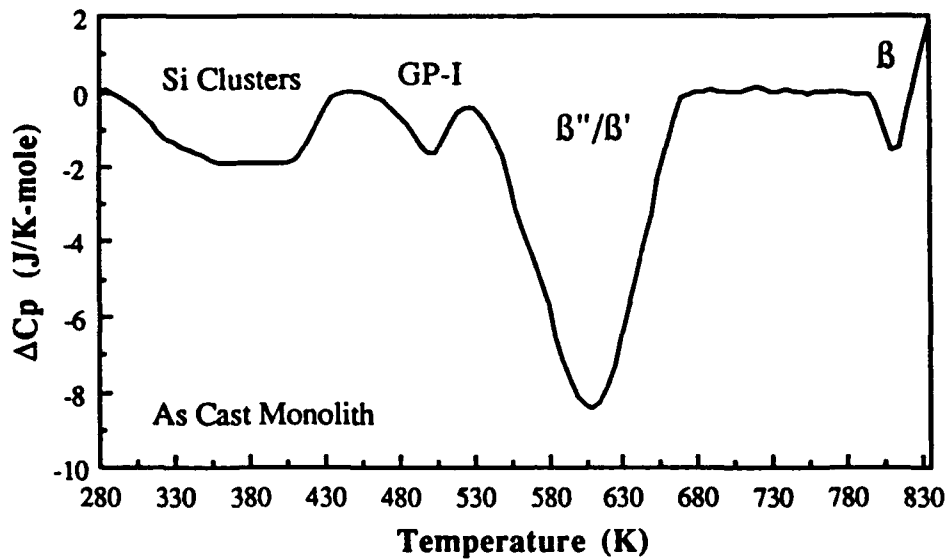


Figure 12: DSC Thermogram of As Cast A356 Al Alloy.

closely to the precipitation sequence for Al-Mg-Si alloys [Ref. 12]. Based on the results of reference 8, which studied precipitation in 6061 Al, the exothermic peaks observed in Figure 12 can be identified as Si cluster, GP-I, GP-II (β'') and β' doublet, and β formation, respectively. The final rise is the beginning of an endothermic β dissolution peak. Since the transition precipitate GP-I zones, β'' and β' constitute the primary hardening constituents in Al-Mg-Si alloys, the following discussion is base on the portion of the thermogram containing the GP-I through β' exotherms.

a. *Effect of SiC Particle Addition on the Matrix Aging Response*

Figure 13 shows the DSC thermograms of the SiC particulate reinforced MMC and the monolithic alloy. Both the GP-I zone formation peak and the peak corresponding to β'' and β' precipitation have been accelerated in the MMC when compared to the monolith, with β' precipitation showing more acceleration. The higher

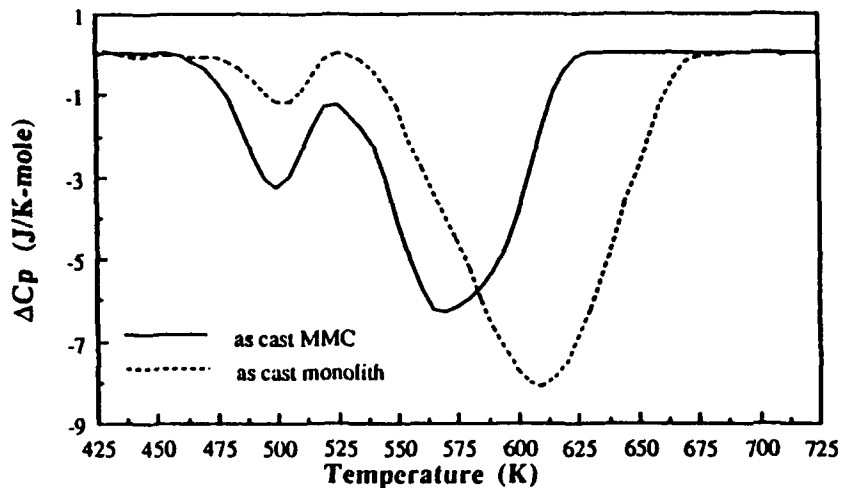


Figure 13: Comparison of As Cast A356 Monolith and MMC.

dislocation density of the MMC matrix provides a larger density of heterogeneous nucleation sites for β''/β' , resulting in a reduced incubation time and a higher nucleation rate [Refs. 15,20], and hence a large acceleration. Additionally, enhanced solute diffusivity through dislocation pipes may also result in acceleration of aging [Ref. 18].

The GP-I zones, on the other hand, grow from Si clusters which nucleate on quenched in vacancy loops [Refs. 12,21]. Since the density of quenched in vacancy loops in the composite matrix is expected to be lower than that in the monolith due to absorption of vacancies at interfacial dislocations, no significant acceleration of the GP-I zone peak is observed due to SiC_p addition.

The relative amount of GP-I zones is seen to be greater in the MMC. For the growth of GP-I zones, only short range diffusion of Mg atoms to the Si vacancy clusters is necessary. On the contrary, formation of β''/β' requires long range migration of solute atoms, and because of the intrinsically low vacancy concentration in the MMC

matrix, growth of β''/β' may be slowed. As a result, the growth of GP-I zones, which form competitively with β'' [Ref. 18], may be favored over that of β'' , resulting in a relatively larger volume fraction of GP-I zones and a smaller volume fraction of β''/β' in the MMC, as compared to the monolith.

b. Effect on Post-Fabrication Processing on the Matrix Aging Response

DSC thermograms of the as cast and as processed A356 Al alloy are shown in Figure 14. GP-I zone formation is seen to be greater in the processed

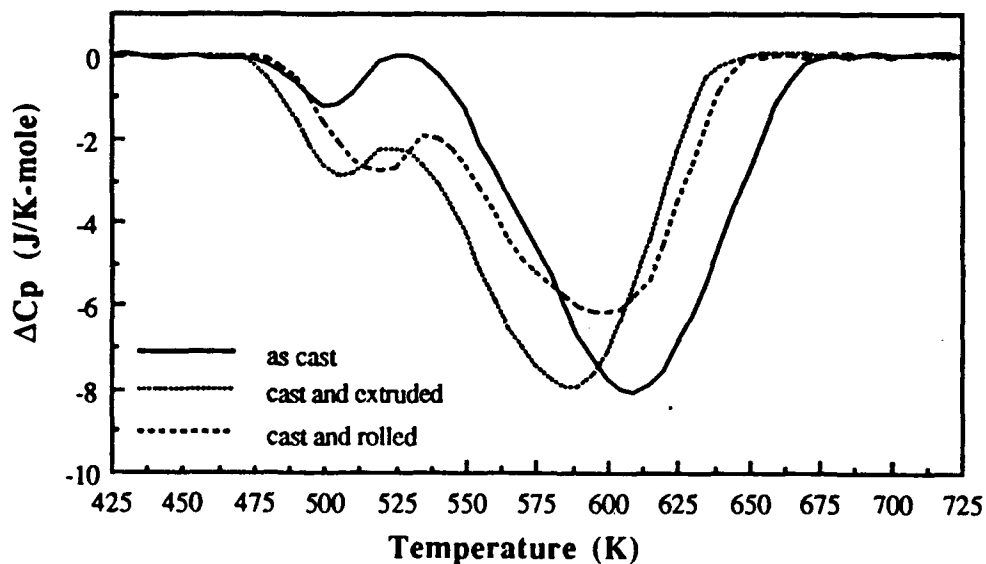


Figure 14: DSC Thermogram of A356 Al Monolith in As Cast, Cast and Extruded, and Cast and Rolled Conditions.

conditions, and it is also delayed due to processing. β''/β' precipitation is greatly accelerated by processing, more so due to extrusion than rolling. It begins before the conclusion of GP-I zone precipitation, as evidenced by the overlapping peaks (superposition of the peaks prevents the thermogram from returning to a 0 ΔC_p value). In comparison, the as cast curve returns to a 0 ΔC_p value prior to beginning β'' precipitation. The extruded specimen shows the greatest β'' precipitation acceleration, followed by the rolled specimen.

Figure 15 shows the results of the DSC scans on the composite materials. It is seen here that GP-I zone formation is delayed as in the monolith.

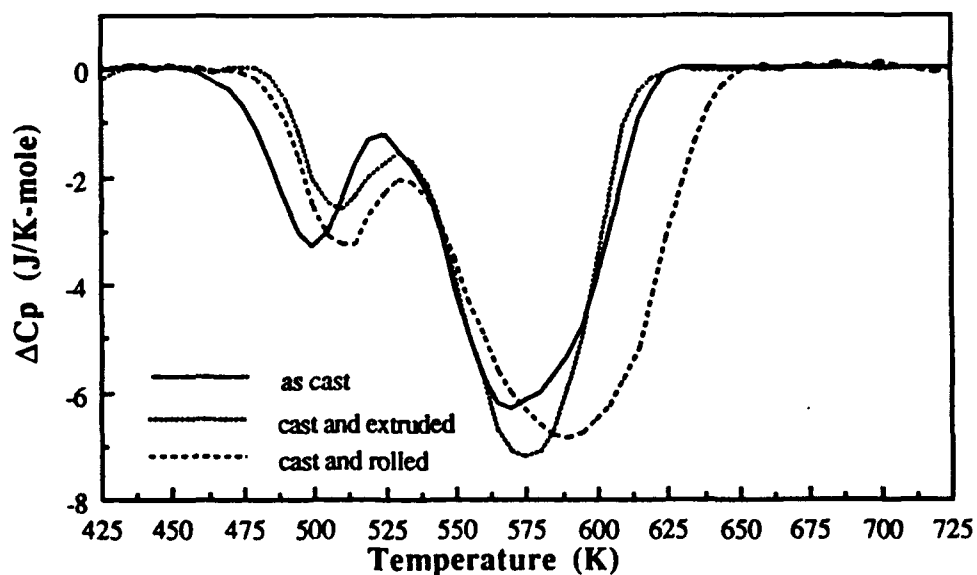


Figure 15: DSC Thermogram of A356 Al MMCs in As Cast, Cast and Extruded, and Cast and Rolled Conditions.

However, the β''/β' peak is also slightly decelerated, contrary to the trend observed in the monolith. As β'' and β' are the primary hardening constituents in A356 Al, these trends are consistent with the microhardness results which showed an acceleration in the monolith, but a slight delay in the MMC.

It is believed that the deceleration in GP-I zone formation due to the extrusion is due to the decrease in vacancy cluster concentration in the extruded material.

The vacancy cluster concentration is lower due to absorption of vacancies at interfacial dislocations as previously described. The acceleration in β''/β' in the monolith is due to an increased density of nucleation sites, i.e., increased dislocation density due to extrusion. It is plausible that the additional deceleration in β''/β' in the composite material is due to recovery of interfacial dislocations to the grain/subgrain boundaries as previously described, decreasing the density of random dislocations available for precipitation within subgrains.

3. Resistivity

Changes in the *in situ* resistivity during aging of the extruded monolith and the as cast and extruded composites are shown in Figures 16 and 17. Figure 16 plots the results of the experiments conducted at an isothermal aging temperature of 428 K. For the extruded materials resistivity increases rapidly at first, commensurate with the formation of Si clusters and/or GP-I zones (segment A-B). Since these precipitates are completely coherent with the matrix, the strain field around the precipitates grows as the precipitates grow.

This higher transformation-induced strain field impedes the flow of electrons more than the removal of solute atoms from the solid solution can assist it. Therefore, there is a rapid rise in resistivity. With continued precipitation, the rate of increase in resistivity decreases, until β''/β' precipitation starts. After another short rise (segment B-C), the resistivity remains fairly constant during β''/β' precipitation.

The plateau represents a regime in which the strain field and solute atom depletion effects roughly equilibrate, keeping the overall resistivity relatively constant.

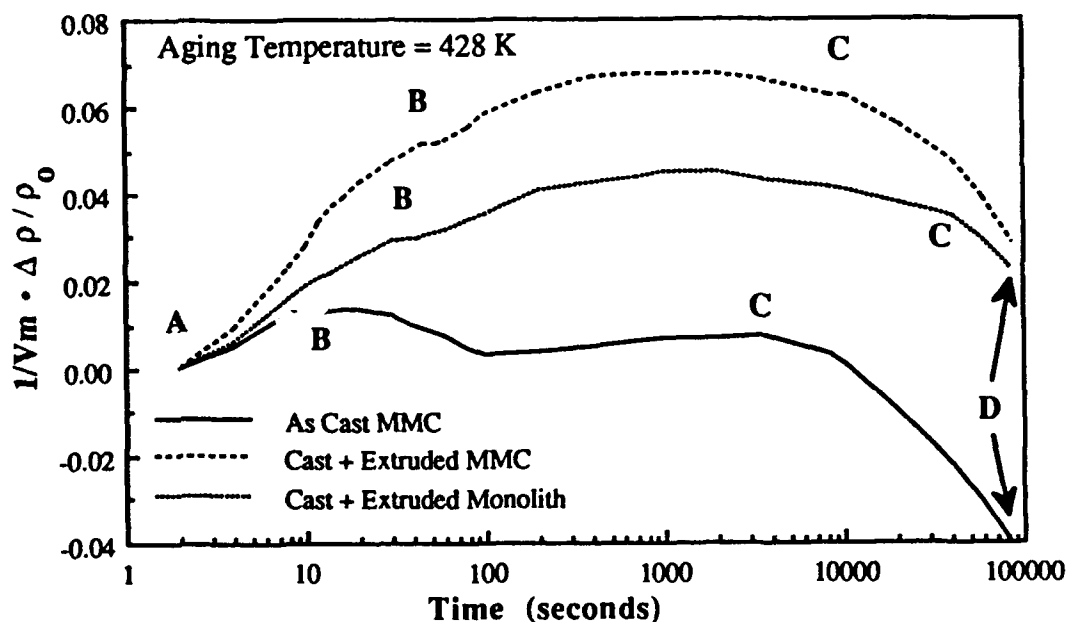


Figure 16: Changes in Resistivity of A356 Al Reinforced with 0 and 26 vol% SiC as a Function of Time at 428K.

As the precipitates coarsen into the semicoherent β' and eventually the incoherent β , the matrix strain decreases, as does the precipitate density. This decrease in strain, coupled with concurrent reductions in the matrix solute content, results in a final net drop of resistivity (segment C-D). [Ref. 18]

The final drop in resistivity due to the $\beta' \rightarrow \beta$ transformation begins in the extruded MMC around 10^4 seconds, while in the extruded monolith it begins around 3×10^4 seconds, indication that β precipitation is accelerated in the MMC. The shorter plateau length prior to final drop (corresponding to β''/β' precipitation) evident in the MMCs indicates accelerated aging, supporting previous results.

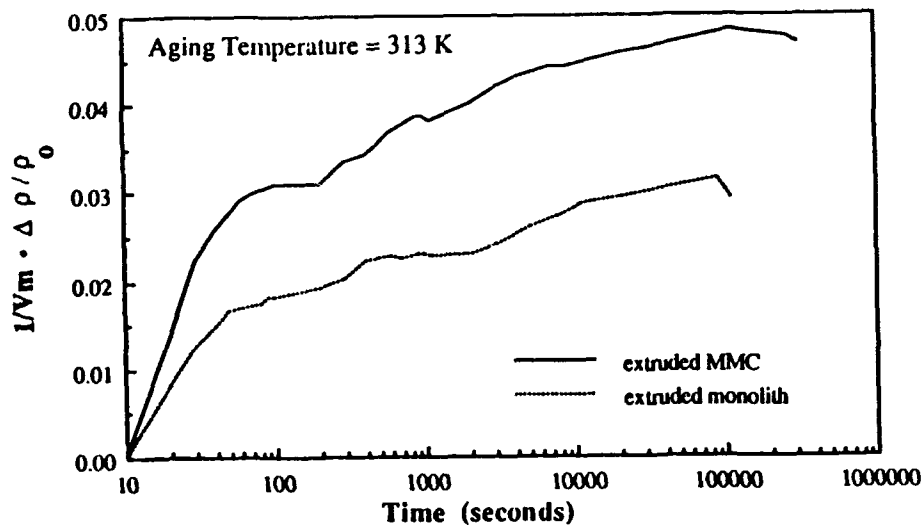


Figure 17: Changes in Resistivity of A356 Al Alloy Reinforced with 0 and 26 vol% SiC as a Function of Time at 313K.

The resistivity of the as cast material does not continue to increase after GP-I zone formation, but rather decreases prior to reaching a plateau, followed by another decrease. It is unclear if the decrease in resistivity following GP-I zone formation is due to quicker solute depletion, or less matrix strain. More research into this behavior is necessary.

Figure 17 depicts the changes in the *in situ* resistivity during aging of the extruded monolith and the extruded composite samples at an isothermal aging temperature of 313 K. Both materials show the same trends in resistivity. At this aging temperature, the increases in resistivity due to Si clustering and GP-I zone precipitation can be individually discerned. The initial rise is considered to be Si clustering, as GP-I zone formation did not occur until much later during heating in the DSC, and the GP-I

zones require a longer time at this temperature to form. The latter rise is due to GP-I zone formation.

It is observed in Figure 17 that the resistivity increases more rapidly initially due to Si-clustering in the composite than in the monolith, suggesting that the rate of nucleation of Si clusters is enhanced in the MMC, probably due to enhanced density of interfacial dislocations. Additionally, the GP-I zone formation is observed to initiate earlier in the MMC relative to the monolith, although this acceleration is not very large.

V. CONCLUSIONS

Centrifugal casting can be effectively utilized to manufacture large composite parts comprising surfaces of revolution. The mechanical properties of castings produced by this process can be substantially improved by thermo-mechanical processing.

The presence of SiC particulates results in substantial refinement of the Si platelets in the A356 Al matrix alloy via eutectic modification. In spite of the presence of SiC, this eutectic modification prevents the ductility of the metal matrix composite from falling far short of the control alloy.

Post-fabrication extrusion reduces the hardness of the solution treated material. This softening is most likely due to a highly refined grain/subgrain structure which allows dislocations generated at the reinforcement/matrix interface to recover to the grain/subgrain boundaries.

Each step in the aging behavior of A356 Al is accelerated due to the addition of SiC, although to different degrees. The primary hardening constituent phases β''/β' experienced the greatest acceleration, with GP-I zones being only slightly accelerated.

The effect of post-fabrication processing on the aging response of the monolith and the composite are quite different. While processing accelerates aging in the monolith, it decelerates the formation kinetics of β''/β' in the MMC. Processing decelerates GP-I zone formation in both the monolith and the composite.

The age hardenability of A356 Al was decreased slightly due to the addition of SiC. Post-fabrication processing also had a greater effect on the age hardenability of the monolith than on that of the composite. While the change to peak hardness in the monolith decreased from 25% to 21% upon extrusion, the change to peak hardness of the MMC remained nearly constant at 19%.

LIST OF REFERENCES

1. Dutta, I., Tiedemann, C.F., and McNelley, T.R., "Effect of Hot Working on the Microstructure and Properties of a Cast 5083 Al-SiC_p Metal Matrix Composite", *Scripta Metallurgica*, Vol. 24, No. 7, pp. 1233-1235, 1990.
2. McNelley, T.R., and Kalu, P.N., "The Effects of Thermomechanical Processing on the Ambient Temperature Properties and Aging Response of a 6061 Al-Al₂O₃ Composite", *Scripta Metallurgica*, Vol. 25, pp. 1041-1046, 1991.
3. Kalu, P.N., and McNelley, T.R., "Microstructural Refinement by Thermomechanical Treatment of a Cast and Extruded 6061 Al-Al₂O₃ Composite", *Scripta Metallurgica*, Vol. 25, pp. 853-858, 1991.
4. Edwards, G.R., and Sherby, O.D., "Influence of Processing History on the Mechanical Behavior of a Zn-W Composite", *International Journal of Powder Metallurgy*, Vol. 7, pp. 21-33, 1971.
5. Edwards, G.R., McNelley, T.R., and Sherby, O.D., "Diffusion-controlled Deformation of Particulate Composites", *The Philosophical Magazine*, Vol. 32, No. 6, pp. 1245-1264, December 1975.
6. *Metals Handbook*, 10th Edition, Vol. 2, ASM International, 1990.
7. Thomas, G., "The Aging Characteristics of Aluminium Alloys", *Journal of the Institute of Metals*, Vol. 90, pp. 57-63, 1961-62.
8. Lutts, A., "Pre-Precipitation in Al-Mg-Ge and Al-Mg-Si", *Acta Metallurgica*, Vol. 9, pp. 577-586, June 1961.
9. Cordier, H. and Gruhl, W., "Beitrag zur Frage der Entmischung bei AlMgSi-Legierungen aufgrund elektronenmikroskopischer Beobachtungen", *Zeitschrift für Metallkunde*, Vol. 56, pp. 669-674, 1965.
10. Ceresara, S., Di Russo, E., Fiorini, P., and Giarda, A., "Effect of Si Excess on the Aging Behavior of Al-Mg₂Si 0.8% Alloy", *Material Science and Engineering*, Vol. 5, pp. 220-227, 1960/70.

11. Kovacs, I., Lendvai, J., and Nagy, E., "The Mechanism of Clustering in Supersaturated Solid Solutions of Al-Mg₂Si Alloys", *Acta Metallurgica*, Vol. 20, pp. 975-983, July 1972.
12. Dutta, I., and Allen, S.M., "A Calorimetric Study of Precipitation in Commercial Aluminium Alloy 6061", *Journal of Materials Science Letters*, Vol. 10, pp. 323-326, 1991.
13. Dutta, I., Bourell, D.L., and Latimer, D., "A Theoretical Investigation of Accelerated Aging in Metal-Matrix Composites", *Journal of Composite Materials*, Vol. 22, pp. 829-849, September 1988.
14. Nieh, T.G., and Karlak, R.F., "Aging Characteristics of B₄C-Reinforced 6061-Aluminum", *Scripta Metallurgica*, Vol. 18, No. 1, p. 25, 1984.
15. Christman, T. and Suresh, S., "Microstructural Development in an Aluminum Alloy-SiC Whisker Composite", *Acta Metallurgica*, Vol. 36, No. 7, pp. 1691-1704, 1988.
16. Dutta, I. and Bourell, D.L., "A Theoretical and Experimental Study of Aluminum Alloy 6061-SiC Metal Matrix Composite to Identify the Operative Mechanism for Accelerated Aging", *Material Science and Engineering A*, Vol. A112, pp. 67-77, 1989.
17. Harper, C.P., "Effect of Alumina Particle Additions on the Aging Kinetics of 2014-Aluminum Matrix Composites", Master's Thesis, Naval Postgraduate School, Monterey, California, September 1991.
18. Dutta, I., Allen, S.M., and Hafley, J.L., "Effect of Reinforcement on the Aging Response of Cast 6061 Al-Al₂O₃ Particulate Composites", *Metallurgical Transactions A*, Vol. 22A, pp. 2553-2563, November 1991.
19. Dutta, I. and Bourell, D.L., "Influence of Dislocation Density and Distribution on the Aging Behavior of 6061 Al-SiC_w Composites", *Acta Metallurgica*, Vol. 38, No. 11, pp. 2041-2049, 1990.
20. Papazian, J.M., "A Calorimetric Study of Precipitation in Aluminum Alloy 2219", *Metallurgical Transactions A*, Vol 12A, pp 269-280, February 1981.
19. Ozawa, E. and Kimura, H., "Excess Vacancies and the Nucleation of Precipitates in Aluminum-silicon Alloys", *Acta Metallurgica*, Vol. 18, pp. 995-1004, September 1970.

INITIAL DISTRIBUTION LIST

- | | | |
|----|---|---|
| 1. | Defense Technical Information Center
Cameron Station
Alexandria, VA 22304-6145 | 2 |
| 2. | Library, Code 0142
Naval Postgraduate School
Monterey, CA 93943-5002 | 2 |
| 3. | Dr. A. P. Direcka
Code R32
Naval Surface Warfare Center, White Oak
Silver Spring, MD 20903 | 1 |
| 4. | Dr. S. D. Karmarkar
Code R32
Naval Surface Warfare Center, White Oak
Silver Spring, MD 20903 | 1 |
| 5. | Professor I. Dutta, Code ME/Du
Naval Postgraduate School
Monterey, CA 93943-5000 | 1 |
| 6. | Christopher W. May
1013 Yacht Court
New Bern, NC 28560 | 1 |